J Biomol NMR (2012) 53:139–148
DOI 10.1007/s10858-012-9631-8

ARTICLE

4D Non-uniformly sampled HCBCACON and $^{1}J(NC^{\alpha})$-selective HCBCANCO experiments for the sequential assignment and chemical shift analysis of intrinsically disordered proteins

Jiří Nováček · Noam Y. Haba · Jordan H. Chill · Lukáš Žídek · Vladimír Sklenář

Received: 16 February 2012 / Accepted: 11 April 2012 / Published online: 13 May 2012

Abstract A pair of 4D NMR experiments for the backbone assignment of disordered proteins is presented. The experiments exploit ^{13}C direct detection and non-uniform sampling of the indirectly detected dimensions, and provide correlations of the aliphatic proton (H^{α}, and H^{β}) and carbon (C^{α}, C^{β}) resonance frequencies to the protein backbone. Thus, all the chemical shifts regularly used to map the transient secondary structure motifs in the intrinsically disordered proteins (H^{α}, C^{α}, C^{β}, C', and N) can be extracted from each spectrum. Compared to the commonly used assignment strategy based on matching the C^{α} and C^{β} chemical shifts, inclusion of the H^{α} and H^{β} provides up to three extra resonance frequencies that decrease the chance of ambiguous assignment. The experiments were successfully applied to the original assignment of a 12.8 kDa intrinsically disordered protein having a high content of proline residues (26 %) in the sequence.

Keywords Intrinsically disordered proteins · Non-uniform sampling · ^{13}C detection · Chemical shifts · Residual secondary structure · Prolines assignment

Electronic supplementary material The online version of this article (doi:10.1007/s10858-012-9631-8) contains supplementary material, which is available to authorized users.

J. Nováček · L. Žídek (✉) · V. Sklenář
Faculty of Science, NCBR, and CEITEC, Masaryk University, Kamenice 5, 625 00 Brno, Czech Republic
e-mail: lzidek@chemi.muni.cz

N. Y. Haba · J. H. Chill
Department of Chemistry, Bar Ilan University, Ramat Gan 52900, Israel

Introduction

Intrinsically disordered proteins (IDPs) characterized by polypeptide chains lacking a stable and well defined tertiary structure in an isolated state have been under increased interest of biochemists and structural biologists for the past decade. IDPs comprise considerable part of the eukaryotic proteome and take part in a number of important processes (Dunker et al. 2000; Ward et al. 2004; Billadeau et al. 2006). Besides, it has been recognized that a non-negligible portion of the IDPs is related to serious human diseases (Bussell and Eliezer 2001; Dyson and Wright 2005; Fink 2005; Dunker et al. 2008).

The unusual structural state of IDPs can be characterized by an array of techniques, ranging from simple indirect methods describing their chemical and physical properties, over the techniques providing information on the size or diffusion behavior to spectroscopic methods supplying both structural and dynamic residue level information. Due to its exceptional capacity to describe structural properties at the atomic resolution, multi-dimensional NMR has become a leading tool to study structure-function relationship of IDPs (Dyson and Wright 2004; Eliezer 2007, 2009). Due to the lack of a rigid structure, the strategy applied to the NMR characterization of the IDP architecture differs significantly from the one utilized for the well ordered systems. The chemical shifts obtained in the process of sequential assignment provide the first important insight into the presence of the residual secondary structure motifs along the amino acid sequence. Due to the increased dynamics of unstructured polypeptide chains, ^{1}H–^{1}H NOE data no longer furnish sufficient information, and the structural studies have to rely on other NMR observables. Among them, measurement of the residual dipolar couplings (RDCs), data supplied by relaxation experiments

and by measurements exploiting the attached paramagnetic labels have proven to provide crucial information to map the conformational space of the IDPs (Ganguly et al. 2009; Mukrasch et al. 2009; Salmon et al 2010).

Various strategies for the backbone assignment of the IDPs have been proposed over the past decade. First, approaches originally developed to assign the well ordered systems have been applied (Peti 2001; Yao et al. 2001; Pannetier 2007; Mukrasch et al. 2009; Motáčková et al. 2009); in particular, a combination of several triple resonance experiments that allow the sequential walk by comparing the chemical shifts of the ^{15}N atoms (Panchal 2001; Zweckstetter et al. 2001; Frueh et al. 2006; Sun et al. 2005) or by matching the resonance frequencies of C^{α} and C^{β}, or C' atoms (Sattler et al. 1999; Rovnyak 2004; Pannetier 2007). However, in case of IDPs where the resonance frequencies exhibit only very low dispersion, the application of the classical approach frequently fails. As demonstrated recently, NMR experiments with higher dimensionality ($m > 3$), correlating nearly all resonances of a single amino acid or stretching over several amino acids, represent an efficient alternative. The acquisition of mD NMR spectra allows to resolve peaks even in the cases of overlap of resonance frequencies in conventional 2D/3D spectra (Atreya et al. 2005; Hiller et al. 2007; Narayanan et al. 2010; Kazimierczuk et al. 2010; Motáčková et al. 2010b; Wen et al. 2011; Nováček et al. 2011).

As the measurement of high resolution spectra with higher dimensionality using the standard techniques would impose extremely long, and in practice unattainable measurement times, special approaches utilizing a sparse sampling are required. Those include reduced dimensionality experiments (Szyperski et al. 1993) rooted in the concept of the "accordion" spectroscopy (Bodenhausen and Ernst 1981, 1982), methods based on projections of multi-dimensional spectra (Ding and Gronenborn 2002; Kim and Szyperski 2003; Kupče and Freeman 2003; Hiller et al. 2005), and experiments exploiting true random sampling in the indirect dimensions (Barna et al. 1987; Barna and Laue 1987; Schmieder et al. 1994; Orekhov et al. 2001; Stern et al. 2002; Malmodin et al. 2005; Marion 2006; Kazimierczuk et al. 2006; Coggins and Zhou 2007). Compared to the standard processing protocols of multi-dimensional NMR data based on the Fast Fourier Transform, special processing procedures are needed to calculate the spectra from the incomplete, sparsely sampled data sets (Coggins and Zhou 2007, 2008; Kupče and Freeman 2008; Mobli and Hoch 2008; Kazimierczuk et al. 2010; Orekhov and Jaravine 2011).

In general, the strategies based on the detection of amide protons fall short to provide sequential assignment of polypeptide chains where two or more consecutive prolines are present. However, recent advances in the design of cryogenically cooled probeheads and developments of the assignment methods utilizing the direct detection of ^{13}C nuclei (Bermel et al. 2005, 2006a, b) to study deuterated and intrinsically disordered proteins (Bermel et al. 2006c, 2009a) paved the way for development of experiments capable to overcome this problem.

Here we present two complementary triple resonance experiments, which improve the sensitivity and extend the originally proposed three-dimensional ^{13}C detected (H)CBCACON and (H)CBCANCO (Bermel et al. 2009a) measurements to the fourth proton dimension. As demonstrated, the measured H^{α}, $H^{\beta 2}$, and $H^{\beta 3}$ chemical shifts greatly facilitate resolution of the carbon atoms in polyproline stretches. The experiments provide the sequential assignment even for IDPs with very high degeneracy of the C^{α} and C^{β} chemical shifts. Each experiment yields all the chemical shifts commonly used to probe for (partial) secondary structure characteristics. The experiments were successfully applied to the original assignment of a 12.8 kDa intrinsically disordered protein having high degeneracy in the amino acid sequence.

Materials and methods

Sample preparation

The ^{13}C, ^{15}N-uniformly labeled sample of WIPc has been prepared as follows. The sequence of the residues 407V–503R of the human WIP protein together with N-terminal and C'-terminal poly histidine tags (for the primary sequence of the WIPc construct see Fig. 2) was cloned into a pET28 vector and transformed into BL21 cells. Typically, cells were grown in a 1.5 L culture of enriched M9 medium (Cai et al. 1998), expression was induced with 1 mM IPTG, and purification utilized immobilized metal ion affinity chromatography which provided sufficiently pure WIPc for NMR sample preparation. The final samples used for the NMR measurements consisted of 1.0–1.2 mM WIPc in 10 mM phosphate buffer, pH 5.0, 20 mM NaCl, 10 mM β-mercaptoethanol, and 7 % D_2O.

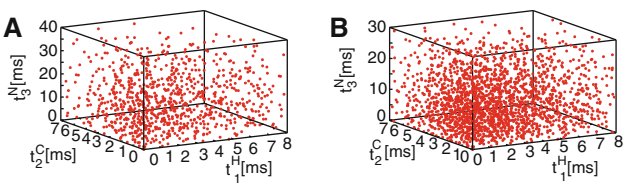

Fig. 1 Graphical representation of 900 indirectly detected time domain points generated using the Poisson disc algorithm used for the acquisition of the 4D HCBCACON (**a**), and of 2,000 indirect points used for the measurement of the 4D $^1J(NC^{\alpha})$-selective HCBCANCO data (**b**)

GSSHHHHHHV DSPRSGPRPP
LPPDRPSAGA PPPPPPSTSI
RNGFQDSPCE DEWESRFYFH
PISDLPPPEP YVQTTKSYPS
KLARNESRSG SNRRERGAPP
LPPIPRLEHH HHHH

Fig. 2 Primary structure of the WIPc construct. The sequence corresponding to the residues 407V–503R of the human WIP protein is depicted in *red*, while the sequence of the N-terminal and C′-terminal poly histidine tags is depicted in *gray*

NMR experiments and data handling

The 4D HCBCACON experiment correlates the resonances of the backbone N of the *i*th amino acid with the H^{α}, H^{β}, C^{α}, C^{β}, and C′ of the $(i-1)$-th amino acid (Fig. 4). The data were measured with the spectral widths set to 6,010 (aq) × 2,000 (N) × 10,000 ($C^{\alpha/\beta}$) × 3,125 ($H^{\alpha/\beta}$) Hz. The maximal acquisition times in the individual indirectly detected dimensions were adjusted to 8 ms for $H^{\alpha/\beta}$, 7 ms for $C^{\alpha/\beta}$, and 40 ms for N dimension. The experiment was acquired with 1,024 complex points in the acquisition dimension and 900 hypercomplex points were randomly distributed (*vide infra*) over the three indirectly detected dimensions. The experiment was acquired based on the parameter set for the standard 2D CON with 8 scans per collected FID. The interscan delay was set to 0.75 s. The data were collected within 31 h which is 0.6 % of the time needed for acquisition of the linearly sample experiment with a similar resolution (25 × 70 × 80 points for $H^{\alpha/\beta}$, $C^{\alpha/\beta}$, N, respectively). The $^{1}J(NC^{\alpha})$-selective HCBCANCO experiment (further denoted as HCBCANCO) correlates the resonance frequency of C′ of the $(i-1)$th amino acid with the H^{α}, H^{β}, C^{α}, C^{β}, and N resonances of the *i*th amino acid (Fig. 4). The experimental data were measured with the spectral widths set to 6,010 (aq) × 2,000 (N) × 10,000 ($C^{\alpha/\beta}$) × 3,125 ($H^{\alpha/\beta}$) Hz. The maximum acquisition times in the individual indirectly detected dimensions were adjusted to 8 ms for $H^{\alpha/\beta}$, 7 ms for $C^{\alpha/\beta}$, and 30 ms for N dimension. The experiment was measured with 1,024 complex points in the directly detected dimension and 2,000 hypercomplex points were randomly distributed in the indirectly detected dimensions. The data were acquired using the parameter set for the standard 2D CON experiment with 8 scans per collected FID and the recovery delay set to 0.75 s. The data were acquired within 69 h, which is equivalent to 1.9 % of the time needed for conventional experiment providing similar resolution (25 × 70 × 60 points for $H^{\alpha/\beta}$, $C^{\alpha/\beta}$, N, respectively). The auxiliary 2D (HCBCA)CON experiment was measured using the pulse code of the 4D HCBCACON, excluding the evolution of the chemical shift in the $H^{\alpha/\beta}$ and $C^{\alpha/\beta}$ dimension. The spectral widths were set to 6,010 (aq) × 2,000 (N) Hz. The total number of 1,024 complex points was measured in the acquisition dimension and 512 complex points in the indirect dimension. The experiment was measured with 8 scans per FID and with the interscan delay of 0.75 s. The non-uniformly sampled HNCACB experiment (Sattler et al. 1999) was measured with spectral widths set to 8,400 (aq) × 2,500 (N) × 10,000 ($C^{\alpha/\beta}$) Hz and the maximal acquisition times 10 ms for $C^{\alpha/\beta}$ and 22 ms for N indirect dimension. The experiment was acquired with 1,024 complex points in the directly detected dimension and 1,300 hypercomplex points in the indirectly detected dimensions. The data were collected with the single scan recovery delay set to 1.15 s and 8 scans per FID. The data were acquired within 17 h, which is equivalent to 23 % of the time needed for conventional experiment providing similar resolution (55 × 100 points for N, $C^{\alpha/\beta}$, respectively). The non-uniformly sampled HNCO experiment (Sattler et al. 1999) was measured with spectral widths set to 8,400 (aq) × 2,000 (N) × 2,000 (C′) Hz. The maximal acquisition times in the individual indirect dimensions were adjusted to 80 ms for N and 50 ms for C′. The experiment was acquired with 2,048 complex points in the directly detected dimension and 500 hypercomplex points in the indirectly detected dimensions. The data were collected with the single scan recovery delay set to 1.0 s and 4 scans per FID. The data were collected within 3 h which is 3 % of the time needed for acquisition of the linearly sample experiment with a similar resolution (160 × 100 points for N, C′, respectively). All data were acquired on a 600 MHz Bruker Avance II spectrometer equipped with the Bruker $^{1}H/^{13}C/^{15}N$ TCI cryogenic probehead with the z-axis gradients at 25°C.

The 4D HCBCACON and HCBCANCO experiments were acquired with the non-uniform sampling of the indirectly detected dimension. The Poisson disc algorithm was

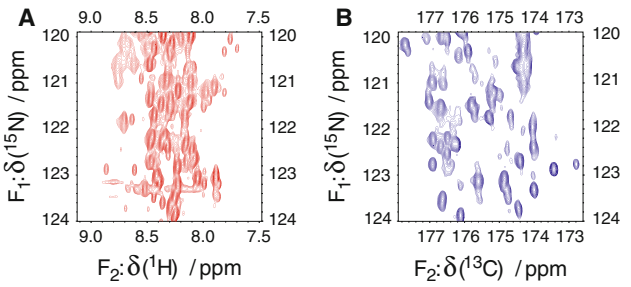

Fig. 3 The central regions of $^{1}H,^{15}N$-HSQC (**a**) and ^{13}C-detected 2D CON (**b**) spectra of the WIPc construct measured on the 600 MHz spectrometer. The spectral widths in the direct dimension were chosen so that the average signal widths (21 Hz for amide protons and 17 Hz for carbonyl ^{13}C, defined as FWHH) appear identical in both plots. Amide proton signals spread over 600 Hz, while the carbonyl signals cover the range of 1,200 Hz in the $^{1}H,^{15}N$–HSQC and 2D CON spectrum, respectively

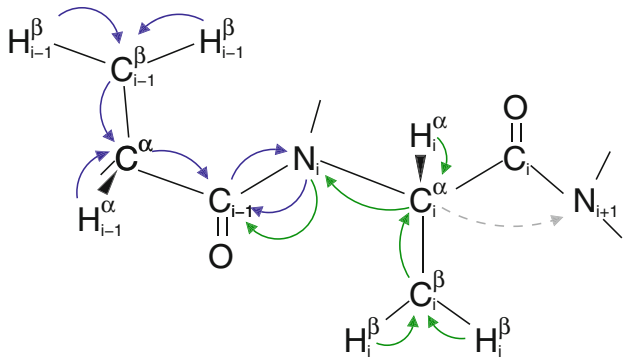

Fig. 4 Magnetization transfer pathways within 4D HCBCACON experiment (*blue arrows*) and 4D $^{1}J(NC^{\alpha})$-selective HCBCANCO experiment (*green arrows*). The *arrows* indicate individual coherence transfer steps via scalar couplings. Transfer via the $^{2}J(NC^{\alpha})$ coupling (*gray arrow*) is actively suppressed within the HCBCANCO experiment

used to generate the time schedule (Kazimierczuk et al. 2008). The algorithm contains a criterion that defines minimal distances between the time points and generates an off-grid sampling scheme. The minimal distance can be represented by an ellipsoid drawn around each time point with the individual radii defined as

$$a_k = \frac{\alpha}{\sqrt[3]{4N\sqrt{2}}}\sqrt{\frac{\mathrm{SW}_l \cdot t_l^{\max} \cdot \mathrm{SW}_m \cdot t_m^{\max}}{(\mathrm{SW}_k \cdot t_k^{\max})^2}}, \qquad (1)$$

where α, N, $\mathrm{SW}_{k,l,m}$, and $t_{k,l,m}^{\max}$ are: factor regulating the discrepancy of generated points ($\alpha = 0.8$), total number of generated time points, spectral width, and maximal evolution time for indirect dimensions, respectively. Symbols k, l, m loop over individual indirectly detected dimensions ($k \neq l \neq m$). At the end, the density of the time points was changed to correspond to the Gaussian distribution ($\sigma = 0.5$). The graphical representation of the sampling schedules used in the present application is shown in Fig. 1.

The uniformly sampled 2D (HCBCA)CON experiment was processed using the spectral processing and analysis system NMRPipe/NMRDraw 3.0 (Delaglio et al. 1995). The non-uniformly sampled 4D HCBCACON and HCBCANCO data were processed using the Sparse Multidimensional Fourier Transform (SMFT) algorithm (Kazimierczuk et al. 2010). The number of spectral points was set to 1,024 in ω_1 ($H^{\alpha/\beta}$) and ω_2 ($C^{\alpha/\beta}$) dimensions for both experiments. All the spectra were analyzed in the graphical NMR assignment and integration software Sparky 3.115 (T. D. Goddard and D. G. Kneller, University of California, San Francisco, USA).

Results and discussion

The interaction between two proteins found exclusively in human T-cells, Wiskott-Aldrich syndrome protein (WASP) and its binding partner WASP-inhibiting protein (WIP) plays a central role in the cytoskeletal changes, particularly actin polymerization, which accompanies T-cell activation (Billadeau et al. 2006). Mutations which perturb formation of the WIP/WASP are responsible for the Wiskott-Aldrich syndrome (WAS) and X-linked thrombocytopenia (XLT), hereditary immunodeficiencies characterized by impaired cytoskeleton formation and an increased incidence of autoimmune diseases and malignancies (Derry et al. 1994). WIP stabilizes WASP by shielding it from the cellular degradation systems and also conveys it to areas of active actin assembly following antigen-receptor and chemokine receptor signaling (Sasahara et al. 2002; de la Fuente et al. 2007). The WIP interaction epitope has been localized to a 35-residues segment at its C-terminal, which has been determined to wrap around the N-terminal WASP EVH1 domain in forming the complex between them (Volkman et al. 2002; Peterson et al. 2007). WIP is predicted to be disordered in solution, and characteristically contains several candidate epitopes which may interact with additional proteins. Thus the unbound state of WIP, yet to be structurally investigated, is biologically relevant.

We have successfully expressed and purified a polypeptide corresponding to residues 407–503 of WIP, henceforth referred to as WIPc (Fig. 2). This region includes a proline-rich domain (residues 413–433, PRD1), the central verprolin conserved region (residues 448–478, VCR), the PKCΘ consensus sequence (residues 485–490) and a C-terminal second proline-rich domain (residues 495–503, PRD2). VCR is common to the verprolin family (60–65 % homology among WIP, WIP-related protein and CR16) and contains the previously established three WASP-binding epitopes (Peterson et al. 2007). Due to its unfolded nature, WIPc cannot be studied using crystallographic methods. Therefore, the multidimensional NMR provides an ultimate tool to characterize the WIPc protein at the atomic resolution. As in the case of other IDPs, the proton dimension of a fingerprint ^{1}H–^{15}N HSQC spectrum (Fig. 3a) exhibits only a very low resolution. To overcome this obstacle and to offset a high occurrence of the proline residues (26 %), experiments relying on the direct ^{13}C detection of carbonyl atoms were used to obtain the sequential assignment of WIPc. In contrast to the ^{1}H–^{15}N HSQC, the ^{13}C detected 2D CON experiment (Bermel et al. 2005) provided a well resolved spectrum exhibiting 92 of the expected 97 correlation peaks. The comparison of resolution in the ^{1}H and ^{13}C detected spectra, with the ranges of the C' and H^{N} resonance and their average line-widths taken into account, showed a 2.4 times higher resolution gained by employing the ^{13}C direct detection of carbonyl resonances (Fig. 3b). Hence, the assignment was first attempted using a standard set of 3D CANCO, CBCACON, and CBCANCO spectra (Bermel

et al. 2006c, 2009a, b). These data provide correlations of each $13C'_i, N_{i+1}$ moiety to its four neighboring (i) and ($i + 1$) $^{13}C^{\alpha}/^{13}C^{\beta}$ nuclei. However, as a consequence of the highly repetitive amino acid sequence, this approach allowed assignments of less than 50 % of the observed resonances despite the favorable resolution in the 2D CON spectra. A close inspection of the primary structure (Fig. 2) shows that WIPc contains 26 % Pro and 15 % Ser in its 97 residues. Besides, WIPc is rich in amino acids with almost identical chemicals shifts of the $^{13}C^{\alpha}/^{13}C^{\beta}$ nuclei, such as Arg, Glu, and His (18 % in total, including the two His-tags) and Asp and Leu (9 %). Such a high content of the amino acids of the same type increases the probability of the signal overlap in the spectra.

To overcome the problem with the high $^{13}C^{\alpha}/^{13}C^{\beta}$ chemical shift degeneracy, we have developed two complementary 4D experiments, HCBCACON and HCBCANCO, that employ the evolution of the chemical shifts of the H^{α} and H^{β} and provide up to three extra resonance frequencies that significantly reduce the chance of ambiguous sequential assignments. The experiments are particularly useful when (1) the matching $^{13}C^{\alpha}$ and $^{13}C^{\beta}$ frequencies are difficult to find due to a high content of amino acids with very similar $^{13}C^{\alpha}$ and $^{13}C^{\beta}$ chemical shifts, (2) high content of prolines further increases the number of frequencies that can be employed in the sequential assignment, as the $^{1}H^{\beta 2}$ and $^{1}H^{\beta 3}$ resonances are well resolved, and (3) the polypeptide chain is flexible and the inherently lower sensitivity of the ^{13}C-detected experiments is partly retrieved by a slower transverse relaxation. The correlation and pulse schemes of the 4D HCBCACON and $^{1}J(NC^{\alpha})$-selective HCBCANCO experiments are shown in Figs. 4 and 5, respectively. Both experiments start with the excitation and chemical shift evolution of $^{1}H^{\alpha}/^{1}H^{\beta}$ protons followed by the $^{1}H^{\alpha}/^{1}H^{\beta} \rightarrow ^{13}C^{\alpha}/^{13}C^{\beta}$ polarization transfer. Optimization of the proton longitudinal relaxation to speed up the acquisition (Pervushin 2002) is achieved by application of a refocused INEPT transfer step referred to as the "H-flip" where an additional 90° pulse is used to return all protons to the equilibrium state (Bermel et al. 2009b). In our implementation, the 180° high power pulse, refocusing the evolution of the ^{1}H–^{15}N scalar interaction during the ^{15}N–$^{13}C'$ evolution, is paired with another 180° pulse with the opposite phase to achieve a net zero effect on the proton magnetizations. This optimization of the proton longitudinal relaxation allowed us to reduce the recycling delay by a factor of 1.7 compared to the experiment without the "H-flip" where a continuous proton decoupling was applied for the same purpose.

The transfer of polarization during the 4D HCBCANCO experiment (Figs. 4b, 5b) has to be confined within a single residue to provide solely intra-residual correlations, reduce the number of correlation peaks, and maximize the sensitivity. This can be achieved by inserting an extra element to eliminate or largely suppress transfer of the magnetization via two-bond $^{2}J(N_{i+1}C_i^{\alpha})$ scalar interactions (Fig. 5b between the points denoted "a" and "d"). Although conceptually identical to the previously proposed solutions for intra-residual 3D HNCA and COHNCA experiments (Permi 2002; Brutscher 2002; Nietlispach et al. 2002), the practical arrangement in the current implementation using the ^{13}C detection of carbonyl atoms differs as only one-directional magnetization transfer $H^{\alpha/\beta} \rightarrow C^{\alpha/\beta} \rightarrow N \rightarrow C'$ is desired.

The Cartesian product operators (Sørensen et al. 1984) at the point denoted with "a" (Fig. 5b) for the magnetizations originated from the $^{1}H^{\alpha}$, $^{13}C^{\alpha}$ (transfer amplitude α) and $^{1}H^{\beta}$, $^{13}C^{\beta}$ (transfer amplitude β) are given by:

$$\alpha : A_i^y \cos(\pi \cdot J(C^{\alpha}C^{\beta}) \cdot 2\Delta)$$
$$\beta : 2A_i^x B_i^z \sin(\pi \cdot J(C^{\alpha}C^{\beta}) \cdot 2\Delta),$$

where A_i and B_i denote the carbon α and carbon β operators of the ith residue, respectively. The operators evolve under the $^{1}J(NC^{\alpha})$, $^{2}J(NC^{\alpha})$, and $J(C^{\alpha}C^{\beta})$ scalar couplings for the whole period confined by the labels "a" and "d". Further, the $J(C'C^{\alpha})$ coupling is active between the time period "a"–"b" and "c"–"d". In the time point "b", a multiple quantum coherence is created by the 90° pulse on C', and the system is allowed to evolve under the $J(NC')$ coupling. The magnetization is returned to the single quantum state in the time point "c" (see Supporting Information for the cartesian product operators at the points denoted with "b" and "c"). The amplitudes for the desired transfers of magnetizations at the end of the building block (time point "d") are given by

$$\alpha : 2A_i^z N_i^z \cos(\pi \cdot J(C^{\alpha}C^{\beta}) \cdot 2\Delta) \cdot \cos(\pi \cdot J(C^{\alpha}C^{\beta}) \cdot T) \cdot \cdot \sin(\pi \cdot {}^{1}J(NC^{\alpha}) \cdot T) \cdot \sin(\pi \cdot {}^{2}J(NC^{\alpha}) \cdot T)$$
$$\beta : 2A_i^z N_i^z \sin(\pi \cdot J(C^{\alpha}C^{\beta}) \cdot 2\Delta) \cdot \sin(\pi \cdot J(C^{\alpha}C^{\beta}) \cdot T) \cdot \cdot \sin(\pi \cdot {}^{1}J(NC^{\alpha}) \cdot T) \cdot \sin(\pi \cdot {}^{2}J(NC^{\alpha}) \cdot T)$$

whereas the amplitudes of the undesired magnetization transfers are

$$\alpha : 2A_i^z N_{i+1}^z \cos(\pi \cdot J(C^{\alpha}C^{\beta}) \cdot 2\Delta) \cdot \cos(\pi \cdot J(C^{\alpha}C^{\beta}) \cdot T) \cdot \cdot \cos(\pi \cdot {}^{1}J(NC^{\alpha}) \cdot T) \cdot \cos(\pi \cdot {}^{2}J(NC^{\alpha}) \cdot T)$$
$$\beta : 2A_i^z N_{i+1}^z \sin(\pi \cdot J(C^{\alpha}C^{\beta}) \cdot 2\Delta) \cdot \sin(\pi \cdot J(C^{\alpha}C^{\beta}) \cdot T) \cdot \cdot \cos(\pi \cdot {}^{1}J(NC^{\alpha}) \cdot T) \cdot \cos(\pi \cdot {}^{2}J(NC^{\alpha}) \cdot T).$$

Next, the $2A_i^{\alpha}N_i^z$ operators are converted to the $-2A_i^zN_i^y$ (or $2A_i^zN_i^x$ created to achieve quadrature detection in States manner) term which is labeled by the ^{15}N chemical shift during the constant time period $2\Delta_7 = 32$ ms incorporating

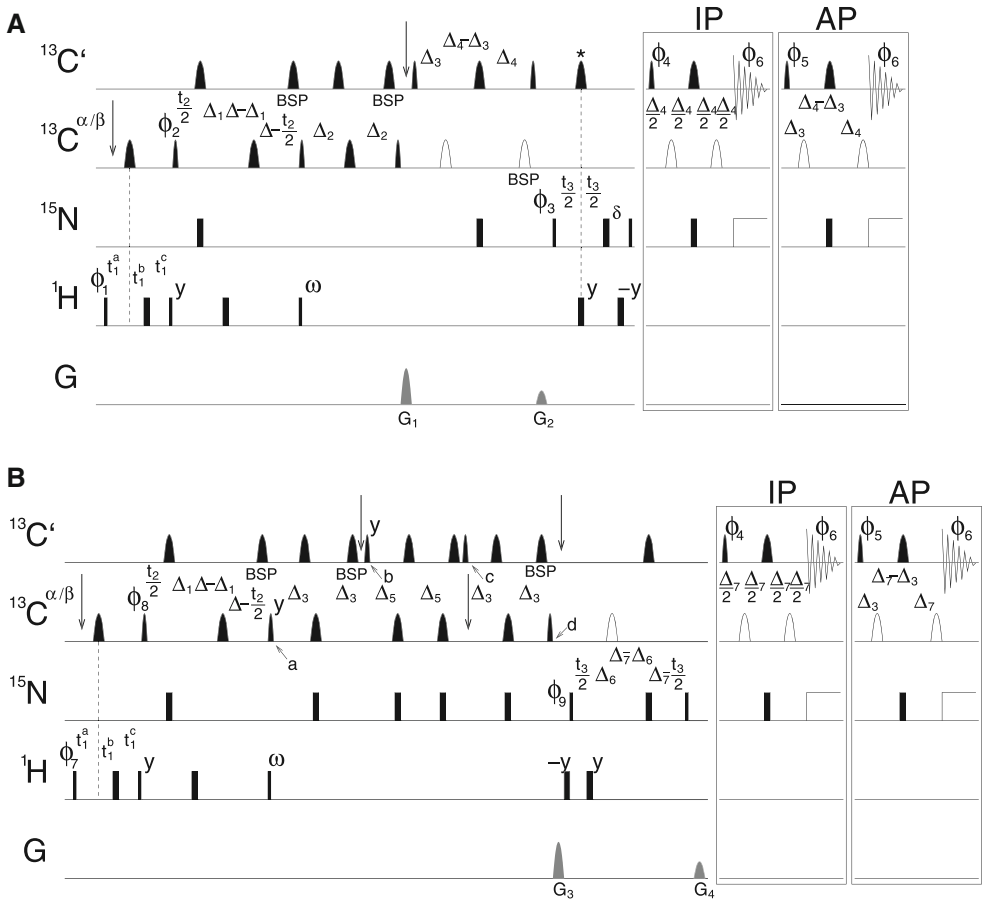

Fig. 5 Pulse sequence scheme of the 4D HCBCACON (**a**) and 4D $^{1}J(\mathrm{NC}^{\alpha})$-selective HCBCANCO (**b**) experiments. The carrier frequencies were placed at 3.0 ppm for ^{1}H, at 44.0 ppm for $^{13}\mathrm{C}^{\alpha/\beta}$, at 123.9 ppm for ^{15}N, and at 175.0 ppm for $^{13}\mathrm{C}'$. The switching of the carrier frequency on the ^{13}C channel is indicated by the *vertical arrows*. The narrow and wide *rectangular shapes* stand for 90° and 180° high power pulses. The narrow and wide filled round symbols represent selective 320 μs 90° Q5 (or time-reversed Q5) and 256 μs 180° Q3 used for $^{13}\mathrm{C}'$ or $^{13}\mathrm{C}^{\alpha/\beta}$ excitation resp. inversion on the 600 MHz spectrometer. The *open round symbols* stand for 256 μs 180° Q3 pulses applied at the center of the $^{13}\mathrm{C}^{\alpha}$ resonance frequency region (58.0 ppm). The *round symbol marked with asterisk* represents an 500 μs adiabatic Chirp pulse used for a simultaneous inversion $^{13}\mathrm{C}'$ and $^{13}\mathrm{C}^{\alpha}$. BSP denotes pulses for compensation of the off-resonance effects. All the pulses were applied with the *x* phase unless noted differently. The IPAP acquisition scheme was implemented to avoid signal splitting in the directly detected dimension due to the $^{13}\mathrm{C}^{\alpha}$-$^{13}\mathrm{C}'$ coupling. The line denoted with G stands for pulsed field gradients applied along the *z*-axis. The *sine-bell shaped* gradients were applied with the following duration and strength: G_1: 1,000 μs, 18 G/cm; G_2: 1,000 μs, 5.4 G/cm, G_3: 1,000 μs, 18 G/cm; G_4: 1,000 μs, 11.4 G/cm. The GARP4 pulse train was employed during the acquisition for ^{15}N decoupling. The following phase cycling was used: $\phi_2 = x, -x$; $\phi_3 = 2(x), 2(-x)$; $\phi_4 = 4(x), 4(-x)$; $\phi_5 = 4(-y), 4(y)$; $\phi_6 = x, 2(-x), x, -x, 2(x), x$; $\phi_8 = y, -y$; $\phi_9 = 2(x), 2(-x)$. The pulse denoted with ω was applied with $-x$ phase and power of the high power pulses for ϕ_1 (ϕ_7) $= x$ or with zero power when the ϕ_1 (ϕ_7) phases were incremented. The initial lengths of the delays were: $\Delta = 3.75$ ms, $\Delta_1 = 1.1$ ms, $\Delta_2 = 3.4$ ms, $\Delta_3 = 4.5$ ms, $\Delta_4 = 12.5$ ms, $\Delta_5 = 15.3$ ms, $\Delta_6 = 11.0$ ms, $\Delta_7 = 16.0$ ms, $t_1^{\mathrm{a}} = 1.8$ ms, $t_1^{\mathrm{b}} = 0.0$ ms, $t_1^{\mathrm{c}} = 1.8$ ms. The evolution of the chemical shift of the $^{1}\mathrm{H}^{\alpha/\beta}$ was performed in the semi-constant time manner incrementing t_1^{a}, t_1^{b}, t_1^{c} delays as follows: $\Delta t_1^{\mathrm{a}} = 1/2\mathrm{SW}, \Delta t_1^{\mathrm{c}} = -t_1^{\mathrm{c}}(0)/\mathrm{TD}, \Delta t_1^{\mathrm{b}} = \Delta t_1^{\mathrm{a}} + \Delta t_1^{\mathrm{c}}$, where SW and TD denote spectral width and number of complex points acquired in the indirect dimension, respectively. The detection of the individual quadrature components of the signal was achieved by incrementation of ϕ_1, ϕ_2, ϕ_3 or ϕ_7, ϕ_8, ϕ_9 in the States manner, respectively

the appropriate time domain incrementation (t_3). Simultaneously, the anti-phase terms $-2\mathrm{A}_i^z\mathrm{N}_i^y$ ($2\mathrm{A}_i^z\mathrm{N}_i^x$) with the amplitudes α and β are refocused with respect to the $^{1}J(\mathrm{NC}^{\alpha})$ coupling and the NC' anti-phase magnetizations are allowed to built up for the subsequent $\mathrm{N} \rightarrow \mathrm{C}'$ transfer. The value of $T = 48.6$ ms for the duration of the whole building block (time points "a"–"d") was found to be optimal for the promotion of the desired transfer. The transfer efficiencies for particular pathways are plotted as functions of the evolution time in Fig. 6a. A comparison of the $\mathrm{C}_i^{\alpha}\mathrm{N}_i$ transfer amplitudes of the originally designed 3D CBCANCO experiment (Bermel et al. 2006c, 2009a) with the 4D $^{1}J(\mathrm{NC}^{\alpha})$-selective HCBCANCO experiment presented here is depicted in Fig. 6b. Neglecting relaxation, the graphs reveal 1.7 times higher efficiency of the transfer amplitude when the two-bond coupling $^{2}J(\mathrm{N}_{i+1}\ \mathrm{C}_i^{\alpha})$ coherence

pathway is suppressed. When the relaxation is considered, the longer evolution imposed by the proposed suppression element lowers this gain and provides improvement of sensitivity only for proteins with $T_2^{\text{eff}} \geq 50.0$ ms.

The implementation of the non-uniform sampling of the indirectly detected dimensions t_1, t_2, and t_3 allowed to extend the maximal acquisition times to 8, 7, and 40 ms, respectively, without a need to increase the number of the indirectly detected points. As a result, 4D spectra with high resolution were obtained within 31 and 69 h for the HCBCACON and HCBCANCO experiments, respectively, representing thus only 0.6 and 1.9 % of the experimental time which would be needed for acquisition of the linearly sampled experiments with a similar resolution.

The non-uniformly sampled data were processed using Sparse Multidimensional Fourier Transform (SMFT) (Kazimierczuk et al. 2009). This method does not recover the full high-dimensional spectrum. Instead, a set of cross-sections with lower dimensionality is calculated at the specific positions of the high-dimensional data set (Kazimierczuk et al. 2010; Zawadzka-Kazimierczuk et al. 2010; Nováček et al. 2011). In case of the 4D HCBCACON and HCBCANCO experiments, a set of $H^{\alpha/\beta}$, $C^{\alpha/\beta}$ 2D cross-sections (Fig. 7) was calculated for all pairs of C'_{i-1}, N_i resonance frequencies identified in the 2D (HCBCA)CON spectrum. Then, the peak picking was performed on the particular cross-sections and the H_i^{α}, $C_i^{\alpha/\beta}$, $H_{i-1}^{\alpha/\beta}$, $C_{i-1}^{\alpha/\beta}$ resonance frequencies were allocated to each C'_{i-1}, N_i correlation signal. Finally, the sequential assignment was performed via matching the $H^{\alpha/\beta}$, $C^{\alpha/\beta}$ resonance frequencies using both a simple UNIX shell script and visual inspection.

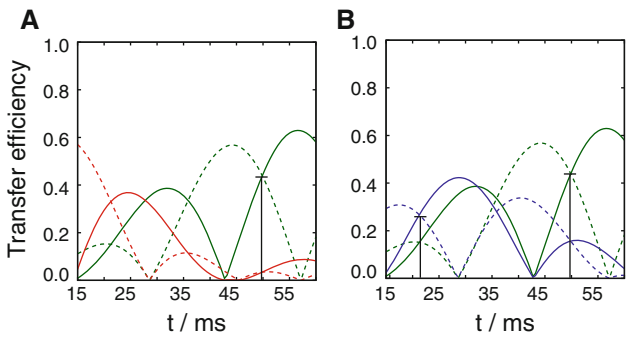

Fig. 6 Transfer efficiencies for the desired (*green solid* and *dashed curves* for the α and β pathway, respectively) and undesired (*red solid* and *dashed curves* for the α and β pathway, respectively) magnetization transfer (**a**). The transfer amplitudes of the $C^{\alpha,i}N^i$ transfer as designed in the original application (*blue solid* and *dashed curves* for the α and β pathway, respectively) (Bermel et al. 2006c, 2009a) and the application proposed here (*green solid* and *dashed curves*) (**b**). The amplitudes corresponding to the applied delay lengths are marked by the *vertical bars*. The values of $^1J(NC^{\alpha}) = 11.0$ Hz, $^2J(NC^{\alpha}) = 7.0$ Hz, $J(C^{\alpha}C^{\beta}) = 35.0$ Hz (Sattler et al. 1999) were used to plot the graphs

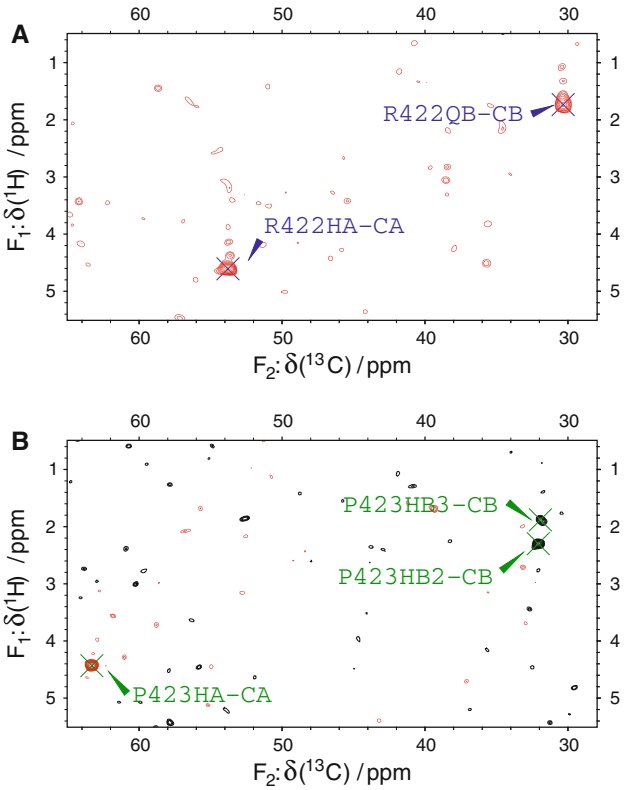

Fig. 7 The examples of the 2D cross-sections from the 4D HCBCACON experiment (**a**) and HCBCANCO experiment (**b**) calculated at the position of the R422C-P423N resonance in the 2D (HCBCA)CON spectrum ($\delta(^{13}C') = 174.024$ ppm, $\delta(^{15}N) = 137.080$ ppm)

Fourier transform of sparsely sampled NMR data leads to processing artifacts commonly termed as a sampling noise. A number of sophisticated methods have been developed to remove the sampling artifacts (Coggins and Zhou 2007, 2008; Stanek and Koźmiński 2010). None of these methods had to be utilized in the present application providing thus an evidence of a very high sensitivity which allowed us to unambiguously identify the signals in the spectra containing both the thermal and the sampling noise. It has to be noted that a significantly reduced number of correlation peaks due to the suppressed $^2J(N_{i+1}C_i^{\alpha})$ coherence pathway greatly reduced the amount of the sampling noise in the 4D HCBCANCO experiment.

The 2D cross-sections from the 4D HCBCACON (Fig. 7a) and 4D HCBCANCO (Fig. 7b) for signals correlating the R422 carbonyl and P423 nitrogen atoms to their $H^{\alpha/\beta}$ and $C^{\alpha/\beta}$ resonances are shown to manifest simplicity of the analysis. Figure 7b documents a particular usefulness of the proposed experiments for the assignment of proline rich sequences. The proline residues are recognized by well separated $H^{\beta 2}$ and $H^{\beta 3}$ chemical shifts even in IDPs, in contrast to most of other amino acids with two H^{β} protons, where the high mobility of the IDPs causes the H^{β} chemical shift averaging (R422 in Fig. 7a). Since the $H^{\beta 2}$ and $H^{\beta 3}$

chemical shifts in all prolines of WIPc are well distinguished, the full potential of five resolved resonances—$H^{\beta 2}$, $H^{\beta 3}C^{\beta}$, H^{α}, and C^{α}—to provide sequential assignments could have been exploited. As a result, all residues in the WIPc construct containing 26 % proline residues in the primary structure were successfully identified. The analysis of the retrieved chemical shifts also revealed why the assignment using the standard 3D experiments failed. The high content of repetitive sequences in WIPc results in severe clustering of the chemical shifts. The sequential assignments in 3D experiments rely on the resolution of the C^{α} and C^{β} chemical shifts. The combined C^{α} and C^{β} chemical shifts of two amino acids i and j with the most similar frequencies $\Delta_{CC} = \sqrt{(C_i^{\beta} - C_j^{\beta})^2 + (C_i^{\alpha} - C_j^{\alpha})^2}$ were found to be less than 10 Hz for 36 amino acids residues. In contrast, when the H^{α} and H^{β} data measured in the 4D experiments were also included in the combined chemical shift calculations, the differences $\Delta_{HHCC} = \sqrt{(C_i^{\beta} - C_j^{\beta})^2 + (C_i^{\alpha} - C_j^{\alpha})^2 + (H_i^{\beta} - H_j^{\beta})^2 + (H_i^{\alpha} - H_j^{\alpha})^2}$ smaller than 10 Hz were identified for only 5 amino acid residues.

The complete sequential assignment of the WIPc construct was achieved using 4D HCBCACON and 4D HCBCANCO with the exception of residues H402, H403, H404 from the N-terminal His-tag, which did not provide any signal in the 2D CON spectrum. In addition, the 4D HCBCANCO spectrum lacked some of the $H^{\alpha/\beta}$, $C^{\alpha/\beta}$ resonance frequencies of residues W450-E451-S452. We attribute this to decreased backbone dynamics in this region, suggested by the fact that peaks corresponding to the 446–456 segment were considerably broadened in the 2D CON spectrum. We were able to overcome this in straightforward manner using the more sensitive proton-detected 3D HNCACB and HNCO experiments which with the benefit of the available 97 % assignment afforded the missing $C^{\alpha/\beta}$ chemical shifts. In contrast to somewhat less-sensitive 4D HCBCANCO, the 4D HCBCACON experiment provided all chemical shifts needed for the secondary structure determination from a single spectrum.

Conclusions

Two complementary 4D experiments (HCBCACON, HCBCANCO) for the sequential assignment of intrinsically disordered proteins have been presented. The experiments combine several approaches to minimize the time necessary to acquire the data and maximize the resolution in the spectra ($^{13}C'$ direct detection, non-uniform sampling, longitudinal relaxation optimization, selective $^{1}J(NC^{\alpha})$ transfer). Thanks to the choice of the correlation scheme, the sequential connectivity is encoded in up to five distinct frequencies (H_i^{α}, $H_i^{\beta 3}$, H_i^{α}, C_i^{β}, and C_i^{α}) and the experiments are well suited for the assignment of the proline rich proteins. The fact that all the chemical shifts employed for the secondary structure estimation are obtained from a single spectrum allows to avoid the problem of systematic deviations in the resonance frequencies (e.g., due to the different sample heating) that may occur when multiple spectra are used. The application of the experiments led to a complete sequential assignment of the 12.8 kDa WIPc protein with 26 % of proline residues (BMRB 18265).

Acknowledgments This work was supported by the project "CEITEC - Central European Institute of Technology" from European Regional Development Fund, grant number CZ.1.05/1.1.00/02.0068, (J. N., L. Z., and V. S.) and by the Czech Science Foundation, grant numbers P206/11/0758 (J. N., L. Z., and V. S.). J.H.C. acknowledges the support of a Legacy Heritage personal grant by the Israel Science Foundation. Financial support by the Access to Research Infrastructures activity in the 7th Framework Programme of the EC (Contract 228461, EAST-NMR) for conducting the research is gratefully acknowledged. The project is a part of Joint Research Activity in the 7th Framework program of the EC (BioNMR n. 261863).

References

Atreya H, Eletsky A, Szyperski T (2005) Resonance assignment of proteins with high shift degeneracy based on 5D spectral information encoded in G(2)FT NMR experiments. J Am Chem Soc 127(13):4554–4555

Barna JCJ, Laue ED, Mayger MR, Skilling J, Worrall SJP (1987) Exponential sampling: an alternative method for sampling in two-dimensional NMR experiments. J Magn Reson 73(1):69–77

Barna JCJ, Laue ED (1987) Comparison of conventional and exponential sampling for 2D NMR experiments: application to a 2D NMR spectrum of a protein. J Magn Reson 75:384–389

Bermel W, Bertini I, Duma L, Felli IC, Emsley L, Pierattelli R, Vasos PR (2005) Complete assignment of heteronuclear protein resonances by protonless NMR spectroscopy. Angew Chem Int Ed 44(20):3089–3092

Bermel W, Bertini I, Felli IC, Piccioli M, Pierattelli R (2006) C-13-detected protonless NMR spectroscopy of proteins in solution. Prog Nucl Mag Res Sp 48(1):25–45

Bermel W, Bertini I, Felli I, Lee Y, Luchinat C, Pierattelli R (2006) Protonless NMR experiments for sequence-specific assignment of backbone nuclei in unfolded proteins. J Am Chem Soc 128(12):3918–3919

Bermel W, Bertini I, Felli IC, Kümmerle R, Pierattelli R (2006) Novel ^{1}3C direct detection experiments, including extension to the third dimension, to perform the complete assignment of proteins. J Magn Reson 178(1):56–64

Bermel W, Bertini I, Csizmok V, Felli IC, Pierattelli R, Tompa P (2009) H-start for exclusively heteronuclear NMR spectroscopy: the case of intrinsically disordered proteins. J Magn Reson 198(2):275–281

Bermel W, Bertini I, Felli IC, Piccioli M, Pierattelli R (2009) Speeding up C-13 direct detection biomolecular NMR spectroscopy. J Am Chem Soc 131(42):15339–15345

Billadeau DD, Burkhardt JK (2006) Regulation of cytoskeletal dynamics at the immune synapse: new stars join the actin troupe. Traffic 7(11):1451–1460

Bodenhausen G, Ernst RR (1981) The accordion experiment, a simple approach to three dimensional NMR spectroscopy. J Magn Reson 45:367–373

Bodenhausen G, Ernst RR (1982) Direct determination of rate constants of slow dynamic processes by two-dimensional "accordion" spectroscopy in nuclear magnetic resonance. J Am Chem Soc 104(5):1304–1309

Brutscher B (2002) Intraresidue HNCA and COHNCA experiments for protein backbone resonance assignment. J Magn Reson 156(1):155–159

Bussell R, Eliezer D (2001) Residual structure and dynamics in Parkinson's disease-associated mutants of alpha-synuclein. J Biol Chem 276(49):45996–46003

Cai M, Ying H, Sakaguchi K, Clore GM, Gronenborn AM, Craigie R (1998) An efficient and cost eddective isotope labeling protocol for proteins expressed in shape *Escherichia coli*. J Biomol NMR 11(1):97–102

Coggins BE, Zhou P (2007) Sampling of the time domain along concentric rings. J Magn Reson 184:207–221

Coggins BE, Zhou P (2008) High resolution 4-D spectroscopy with sparse concentric shell sampling and FFT-CLEAN. J Biomol NMR 42(4):225–239

de la Fuente MA, Sasahara Y, Calamito M, Anton IM, Elkhal A, Gallego MD, Suresh K, Siminovitch K, Ochs HD, Anderson KC, Rosen FS, Geha RS, Ramesh N (2007) WIP is a chaperone for Wiskott-Aldrich syndrome protein (WASp). PNAS 104(3):926–931

Ding K, Gronenborn AM (2008) Novel 2D triple-resonance NMR experiments for sequential resonance assignments of proteins. J Magn Reson 156:262–268

Delaglio F, Grzesiek S, Vuister G, Zhu G, Pfeifer J, Bax A (1995) NMRPipe: a multidimensional spectral processing system based on UNIX pipes. J Biomol NMR 6(3):277–293

Derry JM, Ochs HD, Francke U (1994) Isolation of a novel gene mutated in Wiskott-Aldrich syndrome. Cell 78(4):635–644

Dunker AK, Obradovic Z, Romero P, Garner EC, Brown CJ (2000) Intrinsic protein disorder in complete genomes. Genome Inform 11:161–171

Dunker AK, Silman I, Uversky VN, Sussman JL (2008) Function and structure of inherently disordered proteins. Curr Opin Struct Biol 18(6):756–764

Dyson H, Wright P (2004) Unfolded proteins and protein folding studied by NMR. Chem Rev 104(8):3607–3622

Dyson H, Wright P (2005) Intrinsically unstructured proteins and their functions. Nature Rev Mol Cell Biol 6(3):197–208

Eliezer D (2007) Characterizing residual structure in disordered protein states using nuclear magnetic resonance. Methods Mol Biol 350:49–67

Eliezer D (2009) Biophysical characterization of intrinsically disordered proteins. Curr Opin Struct Biol 19(1):23–30

Fink A (2005) Natively unfolded proteins. Curr Opin Struct Biol 15(1):35–41

Frueh DP, Sun ZYJ, Vosburg DA, Walsh CT, Hoch JC, Wagner G (2006) Non-uniformly sampled double-TROSY hNcaNH experiments for NMR sequential assignments of large proteins. J Am Chem Soc 128(17):5757–5763

Ganguly D, Chen J (2009) Structural interpretation of paramagnetic relaxation enhancement-derived distances for disordered protein states. J Mol Biol 390(3):467–477

Hiller S, Fiorito F, Wuthrich K, Wider G (2005) Automated projection spectroscopy (APSY). PNAS 102(31):10876–10881

Hiller S, Wasmer C, Wider G, Wüthrich K (2007) Sequence-specific resonance assignment of soluble nonglobular proteins by 7D APSY-NMR spectroscopy. J Am Chem Soc 129(35):10, 823–10,828

Kazimierczuk K, Koźmiński W, Zhukov I (2006) Two-dimensional Fourier transform of arbitrarily sampled NMR data sets. J Magn Reson 179:323–328

Kazimierczuk K, Zawadzka A, Koźmiński W (2008) Optimization of random time domain sampling in multidimensional NMR. J Magn Reson 192(1):123–130

Kazimierczuk K, Zawadzka A, Koźmiński W (2009) Narrow peaks and high dimensionalities: exploiting the advantages of random sampling. J Magn Reson 205(2):286–292

Kazimierczuk K, Zawadzka-Kazimierczuk A, Koźmiński W (2010) Non-uniform frequency domain for optimal exploitation of non-uniform sampling. J Magn Reson 197(2):219–228

Kim S, Szyperski T (2003) GFT NMR, a new approach to rapidly obtain precise high-dimensional NMR spectra information. J Am Chem Soc 125:1385–1393

Kupče Ē, Freeman R (2003) Projection-reconstruction of three-dimensional NMR spectra. J Am Chem Soc 125:13958–13959

Kupče Ē, Freeman R (2008) Hyperdimensional NMR spectroscopy. Prog Nucl Magn Reson 11:22–30

Malmodin D, Billeter M (2005) Multiway decomposition of NMR spectra with coupled evolution periods. J Am Chem Soc 127(39):13486–13487

Marion D (2006) Processing of ND NMR spectra sampled in polar coordinates: a simple Fourier transform instead of a reconstruction. J Biomol NMR 36(1):45–54

Mobli M, Stern AS, Hoch JC (2008) Spectral reconstruction methods in fast NMR: reduced dimensionality, random sampling and maximum entropy. J Magn Reson 182(1):96–105

Mobli M, Hoch JC (2008) Maximum entropy spectral reconstruction of nonuniformly sampled data. Concepts Magn Reson 32(6): 436–448

Motáčková V, Kubíčková M, Kožíšek M, Grantz-Šašková K, Švec M, Žídek L, Sklenář V (2009) Backbone H-1, C-13, and N-15 NMR assignment for the inactive form of the retroviral protease of the murine intracisternal A-type particle, inMIA-14 PR. Biomol NMR Assignments 3(2):261–264

Motáčková V, Nováček J, Zawadzka-Kazimierczuk A, Kazimierczuk K, Žídek L, Koźmiński W, Sklenář V (2010) Strategy for complete NMR assignment of disordered proteins with highly repetitive sequences based on resolution-enhanced 5D experiments. J Biomol NMR 48(3):169–177

Mukrasch M, Bibow S, Korukottu J, Jeganathan S, Biernat J, Griesinger C, Mandelkow E, Zweckstetter M (2009) Structural polymorphism of 441-residue Tau at single residue resolution. PLoS Biol 7(2):399–414

Narayanan RL, Durr UHN, Bibow S, Biernat J, Mandelkow E, Zweckstetter M (2010) Automatic assignment of the intrinsically disordered protein Tau with 441-residues. J Am Chem Soc 132(34):11906–11907

Nietlispach D, Ito Y, Laue ED (2002) A novel approach for the sequential backbone assignment of larger proteins: selective intra-HNCA and DQ-HNCA. J Am Chem Soc 124:11199–11207

Nováček J, Zawadzka-Kazimierczuk A, Papoušková V, Žídek L, Koźmiński W, Sklenář V (2011) 5D ^{13}C-detected experiments for backbone assignment of unstructured proteins with a very low signal dispersion. J Biomol NMR 50(1):1–11

Orekhov VY, Ibraghimov IV, Billeter M (2001) MUNIN: a new approach to multi-dimensional NMR spectra interpretation. J Biomol NMR 20(1):49–60

Orekhov VY, Jaravine VA (2011) Analysis of non-uniformly sampled spectra with multi-dimensional decomposition. Prog Nucl Magn Reson 59(3):271–292

Panchal SC, Bhavesh NS, Hosur RV (2001) Improved 3D triple resonance experiments, HNN and HN(C)N, for H-N and N-15

sequential correlations in (C-13, N-15) labeled proteins: application to unfolded proteins. J Biomol NMR 20(2):135–147

Pannetier N, Houben K, Blanchard L, Marion D (2007) Optimized 3D-NMR sampling for resonance assignment of partially unfolded proteins. J Magn Reson 186(1):142–149

Permi P (2002) Intraresidual HNCA: an experiment for correlating only intraresidual backbone resonances. J Biomol NMR 23(3):201–209

Pervushin K, Vogeli B, Eletsky A (2002) Longitudinal H-1 relaxation optimization in TROSY NMR spectroscopy. J Am Chem Soc 124(43):12898–12902

Peterson FC, Deng Q, Zettl M, Prehoda KE, Lim WA, Way M, Volkman BF (2007) Multiple WASP-interacting protein recognition motifs are required for a functional interaction with N-WASp. J Biol Chem 282(11):8446–8453

Peti W, Smith LJ, Redfield C, Schwalbe H (2001) Chemical shifts in denatured proteins: resonance assignments for denatured ubiquitin and comparisons with other denatured proteins. J Biomol NMR 19(2):153–165

Rovnyak D, Frueh DP, Sastry M, Sun ZYJ, Stern AS, Hoch JC, Wagner G (2004) Accelerated acquisition of high resolution triple-resonance spectra using non-uniform sampling and maximum entropy reconstruction. J Magn Reson 170(1):15–21

Salmon L, Nodet G, Ozenne V, Yin G, Jensen MR, Zweckstetter M, Blackledge M (2010) NMR characterization of long-range order in intrinsically disordered proteins. J Am Chem Soc 132:8407–8418

Sasahara Y, Rachid R, Byrne MJ, de la Fuente MA, Abraham RT, Ramesh N, Geha RS (2002) Mechanism of recruitment of WASP to the immunological synapse and of its activation following TCR ligation. Mol Cell 10(6):1269–1281

Sattler M, Schleucher J, Griesinger C (1999) Heteronuclear multidimensional NMR experiments for the structure determination of proteins in solution employing pulsed field gradients. Prog Nucl Mang Reson Spect 34(2):93–158

Schmieder P, Stern AS, Wagner G, Hoch JC (1994) Improved resolution in triple-resonance spectra by nonlinear sampling in the constant-time domain. J Biomol NMR 4(4):483–490

Sørensen OW, Eich GW, Levitt MH, Bodenhausen G, Ernst RR (1984) Product operator formalism for the description of NMR pulse experiments. Prog Nucl Mang Reson Spect 16:163–192

Stanek J, Koźmiński W (2002) Iterative algorithm of discrete Fourier transform for processing randomly sampled NMR data sets. J Biomol NMR 47(1):65–77

Stern AS, Li KB, Hoch JC (2002) Modern spectrum analysis in multidimensional NMR spectroscopy: comparison of linear-prediction extrapolation and maximum-entropy reconstruction. J Am Chem Soc 124(9):1982–1993

Sun ZYJ, Frueh DP, Selenko P, Hoch JC, Wagner G (2005) Fast assignment of N-15-HSQC peaks using high-resolution 3D HNcocaNH experiments with non-uniform sampling. J Biomol NMR 33(1):43–50

Szyperski T, Wider G, Bushweller JH, Wütrich K (1993) Reduced dimensionality in triple-resonance NMR experiments. J Am Chem Soc 115(20):9307–9308

Volkman BF, Prehoda KE, Scott JA, Peterson FC, Lim WA (2002) Structure of the N-WASP EVH1 domain-WIP complex: insight into the molecular basis of Wiskott-Aldrich Syndrome. Cell 111(4):565–576

Ward JJ, Sodhi JS, McGuffin LJ, Buxton BF, Jones DT (2004) Prediction and functional analysis of native disorder in proteins from the three kingdoms of life. J Mol Biol 337(3):635–645

Wen J, Wu J, Zhou P (2011) Sparsely sampled high-resolution 4-D experiments for efficient backbone resonance assignment of disordered proteins. J Magn Reson 209(1):94–100

Yao J, Chung J, Eliezer D, Wright PE, Dyson HJ (2001) NMR structural and dynamic characterization of the acid-unfolded state of apomyoglobin provides insights into the early events in protein folding. Biochemistry 40(12):3561–3571

Zawadzka-Kazimierczuk A, Kazimierczuk K, Koźmiński W (2010) A set of 4D NMR experiments of enhanced resolution for easy resonance assignment in proteins. J Magn Reson 202(1):109–116

Zweckstetter M, Bax A (2001) Single-step determination of protein substructures using dipolar couplings: aid to structural genomics. J Am Chem Soc 123(39):9490–9491